Published in final edited form as:
J Am Coll Cardiol. 2009 August 11; 54(7): 638–651. doi:10.1016/j.jacc.2009.03.071.

Mitral cerclage annuloplasty, a novel transcatheter treatment for secondary mitral valve regurgitation: Initial results in swine

June-Hong Kim, MD, **Ozgur Kocaturk, MSc**, **Cengizhan Ozturk, PhD, MD**, **Anthony Z. Faranesh, PhD**, **Merdim Sonmez, MSc**, **Smita Sampath, PhD**, **Christina E. Saikus, BS**, **Ann H. Kim, BS**, **Venkatesh K. Raman, MD, FACC**, **J. Andrew Derbyshire, PhD**, **William H. Schenke, BS**, **Victor J. Wright, BS**, **Colin Berry, PhD, MD**, **Elliot R. McVeigh, PhD**, and **Robert J. Lederman, MD, FACC**

From the Translational Medicine Branch, Division of Intramural Research, National Heart Lung and Blood Institute, National Institutes of Health, Bethesda, MD, USA (all); Cardiology Division, Pusan National University, Busan, Korea (JHK); Department of Biomedical Engineering, Bogazici University, Istanbul, Turkey (CO, MS)

Structured Abstract

Objectives—We developed and tested a novel transcatheter circumferential annuloplasty technique to reduce mitral regurgitation in porcine ischemic cardiomyopathy.

Background—Catheter-based annuloplasty for secondary mitral regurgitation exploits the proximity of the coronary sinus to the mitral annulus, but is limited by anatomic variants and coronary artery entrapment.

Methods—The procedure, “cerclage annuloplasty,” is guided by MRI roadmaps fused with live X-ray. A coronary sinus guidewire traverses a short segment of basal septal myocardium to reenter the right heart where it is exchanged for a suture. Tension is applied interactively during imaging and secured with a locking device.

Results—We found two feasible suture pathways from the great cardiac vein across the interventricular septum to create cerclage. Right-ventricular septal reentry required shorter fluoroscopy times than right atrial reentry, which entailed a longer intramyocardial traversal but did not cross the tricuspid valve. Graded tension progressively reduced septal-lateral annular diameter but not end-systolic elastance or regional myocardial function. A simple arch-like device protected entrapped coronary arteries from compression even during supra-therapeutic tension.

Cerclage reduced mitral regurgitation fraction (from 22.8 ± 12.7% to 7.2 ± 4.4%, p=0.04) by slice-tracking velocity-encoded MRI. Flexible cerclage reduced annular size but preserved annular motion. Cerclage also displaced the posterior annulus towards the papillary muscles. Cerclage introduced reciprocal constraint to the left ventricular outflow tract and mitral annulus that enhanced leaflet coaptation.

A sample of human coronary venograms and CT angiograms suggested that most have suitable venous anatomy for cerclage.

Address for Correspondence: Robert J. Lederman, MD, Translational Medicine Branch, Division of Intramural Research, National Heart Lung, and Blood Institute, National Institutes of Health, Building 10, Room 2c713, Bethesda, MD 20892-1538, USA. Telephone: +1-301-402-6769. Email: ledermar@nhlbi.nih.gov.

Conflicts of Interest and Relationship with industry: JHK, OK, RJL are co-inventors in patent applications related to cerclage and coronary artery protection assigned to NIH.
MS was a student employee of Siemens Corporate Research.

Conclusions—Transcatheter mitral cerclage annuloplasty acutely reduces mitral regurgitation in porcine ischemic cardiomyopathy. Entrapped coronary arteries can be protected. MRI provided insight into the mechanism of cerclage action.

Keywords

Image guided intervention; Catheter-based intervention, non-coronary; Magnetic resonance imaging; Multimodality image fusion

Introduction

Mitral valve regurgitation aggravates symptoms and prognosis in ischemic cardiomyopathy (1,2). Secondary mitral regurgitation caused by annular dilation and subvalvular traction in cardiomyopathy can be corrected by surgical annuloplasty and adjunctive leaflet and subvalvular repair(3,4).

Investigational catheter-based procedures improve valve function in this setting(2). These include devices that shorten or displace the coronary sinus(5–11), trans-cameral fixtures(12–14), endoventricular annular plication(15), sub-papillary interstitial polymer injections(16), and direct leaflet stapling(17–20). Most suffer important limitations compared with surgical repair. Coronary sinus approaches are limited by discordant anatomic planes of the sinus and mitral annulus(21–23); by devices that shorten only a small arc of annular circumference not necessarily encompassing or in-phase with the mitral commissures; and by compression of entrapped left circumflex coronary arteries(21,22,24). Leaflet-stapling procedures constrain leaflet excursion, do not reduce annular dilation, and may exacerbate subvalvular traction(25).

Inspired by epicardial pursestring annuloplasty before the cardiopulmonary bypass era (26), we have developed a novel catheter-based technique to reduce mitral annular circumference. A circumferential “cerclage” suture traverses the coronary sinus and basal septal myocardium and is secured within the right atrium. Cerclage introduces centripetal force uniformly, irrespective of the rotational orientation of the commissures, to enhance mitral leaflet coaptation.

In this paper we address whether cerclage is feasible in swine, whether entrapped coronary arteries can be protected from extrinsic compression, whether cerclage affects mitral regurgitation and mitral annular dynamics in ischemic cardiomyopathy, and what mechanisms appear to underlie cerclage action.

Methods

Animals

Animal experiments were approved by the NHLBI Animal Care and Use Committee. Naïve (healthy) Yorkshire and Yucatan swine (62±17 kg) were used for technical development, and Yucatans (66±23 kg) for cardiomyopathy models. Anesthesia was induced with atropine, butorphanol, ketamine, and xylazine and maintained with inhaled isoflurane and mechanical ventilation.

Ischemic cardiomyopathy was created with serial transcatheter myocardial infarction over 6–8 weeks. Animals were pretreated with amiodarone, atenolol, and aspirin. Target coronary arteries underwent transfemoral balloon preconditioning (10 cycles of 1–2 minutes) followed by undiluted ethanol 1–2 mL through inflated balloons. Ethanol injection was repeated into additional posterolateral coronary branches up to three cycles every 2–4 weeks

until mitral regurgitation was evident on MRI. The average number of infarction procedures was 1.6 over 66 days, with a cumulative mortality of 45% before cerclage. After infarction, animals received topical fentanyl and butorphanol as needed. Animals exhibiting signs of heart failure (57%) received lisinopril and furosemide daily (33%) as needed.

For cerclage, 9Fr introducer sheaths were placed percutaneously into the right jugular and femoral veins, 6Fr introducer sheaths into a femoral artery, and heparin 150 units/kg was administered. After endpoint assessment, animals were euthanized under general anesthesia.

The concept of mitral cerclage annuloplasty

A guidewire loop is created around the mitral annulus and left ventricular outflow tract and then exchanged for a suture [Figure 1]. The guidewire traverses the coronary sinus and the proximal great cardiac vein into the first septal perforator vein towards the basal interventricular septum. It is then directed across a short segment of myocardium under imaging guidance (see supplement) to reenter a right heart chamber where it is ensnared and exchanged for a suture and tension fixation device.

To conduct cerclage, a transjugular balloon-tipped guiding catheter (*Vueport 8Fr*, Cardima) is introduced into the coronary sinus beyond the hemiazygous branch (common in pigs(27)), the occlusion balloon inflated, and a retrograde venogram pressurizes and opacifies the great cardiac vein and septal perforator veins. A 0.014″ guidewire (*MiracleBros 3 or 4.5 or Confianza*, Asahi) is steered using a deflectable microcatheter (*Venture*, St Jude) into the first basal septal perforator vein. Once the targeted right heart chamber is entered, the guidewire is ensnared and replaced with a braided non-absorbable suture. To fix the tension, both suture free ends were externalized and tied beyond a short catheter, which was implanted in a subcutaneous pocket.

Coronary artery protection device

Circumflex coronary artery branches underlie the coronary sinus in most human(21,22,24) and porcine hearts, and are susceptible to compression during coronary sinus annuloplasty. We developed a rigid arch protection device to displace compressive forces away from an entrapped coronary artery [Figure 2]. The device is positioned over the cerclage suture where it crosses the coronary artery, identified by selective coronary arteriography. Suture tension anchors and orients the arch away from the underlying artery. The prototype consists of a length of seamless, annealed, and sinter-polished nitinol alloy hypotube. It has an inner diameter of 1.1 mm, an outer diameter of 1.5mm, a length of 12 mm, and an arch-to-base height of 4mm.

Protection efficacy was measured during graded annuloplasty tension, recording simultaneous aortic and distal coronary artery pressure, using a 0.014″ guidewire pressure transducer (*PressureWire*, Radi Medical Systems). Cerclage annular tension was measured with a digital force meter (ZPH, Imada).

Imaging and Imaging Guidance

Cerclage procedures were guided by X-ray Fused with MRI (XFM), in which MRI-derived roadmaps are registered, with millimeter precision, onto live X-ray using external fiducial markers(28,29). Briefly, 16 multi-modality fiducial marker beads are affixed to the thorax. The markers are identified using three-dimensional T1-weighted gradient echo MRI. Corresponding fiducial markers are identified on MRI and two or three different baseline X-ray projections and registered using closed-form rigid body registration(29).

XFM regions of interest were segmented manually from cardiac MRI, including the interventricular septum, the planned right ventricular endocardial or right atrial endocardial re-entry target for the cerclage guidewire, and right ventricular outflow tract [Figure 1C–E]. These were intended to help the operator maintain an intra-septal course and target suitable right-sided chamber re-entry.

The regions of interest are contoured on an external workstation (*Leonardo*, Siemens) from multiple, breath-held, electrocardiogram (ECG)-gated cine steady-state free precession (SSFP) MRI at end-diastole, described below. X-ray images are captured at 8 frames/s using a video frame grabber (*Accustream 170*, Foresight Imaging) in a separate workstation. Custom fusion software operates in *MATLAB* (Mathworks). After baseline registration, fused images are displayed to the operator alongside live X-ray.

Magnetic resonance imaging

Impact of cerclage on global and regional ventricular function—MRI was conducted at 1.5T (*Sonata or Espree*, Siemens, Erlangen) using standard 4–8 channel Torso array coils. Function was assessed using ECG-gated, segmented, breath-held, balanced SSFP pulse sequences. For geometry and function, typical acquisition parameters were: TR/TE, 3.6/1.8 ms; flip angle, 65°; FOV, 300 mm×244 mm; matrix, 256×127 pixels; slice thickness, 8 mm; bandwidth, 1085 Hz/pixel). Septal-lateral annular and cerclage diameter, and the angle and offset between the annular and cerclage planes were measured in the three-chamber view. The offset, or distance between the coronary sinus and the mitral annulus, was measured orthogonal to the annulus plane(21). Left ventricular wall motion score index was determined using a 16-segment model(30).

Mitral annular dynamics—A basal short axis slice was obtained at the level of the mitral valve annulus after which a stack of long-axis (typically 15) slices 2mm apart were obtained perpendicular to the line of mitral valve coaptation. Typical parameters were voxels, 1.6×1.6×4 mm; flip angle, 50°; views per cardiac cycle, 5; TR/TE, 5/2.5 ms. The annulus and mitral leaflets from the annulus to the line of coaptation were segmented for each frame using semiautomatic tools (Argus, Siemens) and time-resolved three-dimensional leaflet surfaces and least-squares annular paths were reconstructed and further analyzed in *MATLAB* (Mathworks, Inc). Mitral leaflet configuration and traction measurements were recorded as described for echocardiography by Zhu *et al*(31), [Supplementary figure 1]. Mitral leaflet tenting area was recorded as described by Yiu *et al* (32). Annular geometry was recorded as described by Kaji *et al*(33) including commissural and septal-lateral annular width. Annular height was measured from the peak to nadir with relation to the mean annular plane, and normalized by commissural width. Annular area was measured as the three-dimensional surface connecting annular points to the annular centroid. For analysis of annular motion, time-resolved measurements were fitted using a moving-average spline interpolation using the five nearest neighbor points. Reconstructed annulus and leaflets were also overlaid on time-resolved images for visual reference. Displays of time-resolved parameters were normalized for duration of cardiac cycle beginning with the electrocardiogram QRS gating signal.

Velocity encoded MRI—Our laboratory is not consistently successful in measuring mitral valve regurgitation using closed-chest, transthoracic or transesophageal echocardiography. Therefore, we developed custom tools accurately to measure small changes in mitral regurgitation using velocity-encoded MRI with correction for through-plane annular motion in a two-step process.

The time-resolved location and orientation of the mitral valve scan plane was determined from a set of two-dimensional long-axis breathheld, ECG-gated, cine SSFP acquisitions prescribed in a radial arrangement through the mitral valve. Typical imaging parameters were: 320×260mm (81.25% phase) FOV; 1.67×1.67mm (100% phase) resolution; 6mm slice thickness; 80° flip angle, TR/TE=3.02/1.51ms and 930Hz/pixel acquisition bandwidth. An acquisition matrix of 192×160 with 16 views per segment was employed with 48ms temporal resolution and a scan time of 10 R-R intervals. Flow sensitive, two-dimensional breathheld, ECG-gated cine phase-contrast, gradient echo imaging was performed to acquire short axis slices spanning the full-extent of the range of motion of the mitral valve plane that was determined from the previously scanned series. Typical imaging parameters were: 320×220mm (68.75% phase) FOV; 1.67×2.22mm resolution (interpolated to 1.67×1.67mm pixels); 6mm slice thickness incrementally offset each 3mm; 30° flip angle; TR/TE = 6.2/2.8 ms and 440Hz/pixel bandwidth. An acquisition matrix of 192×100 with 5 views per segment each for reference and flow encoding, yielded 62ms temporal resolution. Flow sensitivity (Venc) was optimized for each study, ranging from± 150cm/s to 200cm/s.

Custom semiautomatic analysis software (MATLAB, The MathWorks, Natick, MA, USA) was employed to identify the position and orientation of the mitral valve plane as a function of cardiac phase from the two-dimensional SSFP (anatomical) images, and interpolate the phase-contrast velocity data to obtain a velocity map from a two-dimensional virtual slice that dynamically tracks the mitral valve plane. We also graded mitral regurgitation by radiocontrast ventriculography according to a standard 4-point scale(34).

Color velocity maps with simultaneous tagged MRI were obtained in single breath-held acquisitions using spatial modulation of magnetization with encoded gradients for gauging speed (“SPAMM n’EGGS”)(35).

Impact of cerclage on pressure-volume relationships

End-systolic and end-diastolic pressure-volume relationships were recorded during preload reduction as cerclage tension was varied. Continuous high-fidelity left ventricular pressure and conductance-derived volume signals were obtained using a dedicated instrument (CFL-512, CD Leycom, Zoetermeer, Netherlands) during ventilator-apnea at end-expiration. We calibrated volumes by injecting 10% saline into the pulmonary artery (36). For each tension, data were obtained at steady state and during balloon occlusion of the inferior atriocaval junction (*Coda* 32mm, Cook Medical). Surface electrocardiograms were recorded during cerclage.

Human Imaging for Suitability

We sought evidence from two clinical datasets that humans have septal perforator veins suitable for cerclage. In the first, we reviewed ten anonymized and de-linked coronary venograms obtained during left ventricular pacemaker lead implantation for congestive heart failure (Courtesy of MS Lee and RR Makkar, Cedars-Sinai Medical Center). In the second we analyzed 24 sequential anonymized coronary computed tomography datasets (64 × 0.625mm detector rows (*Brilliance*, Philips)) from ECG-gated breath-held acquisitions (Courtesy of DE Bush and EP Shapiro, Johns Hopkins Bayview Medical Center). These do not constitute human subjects research under US 45CFR§46.102(f).

Statistics

Continuous parameters were compared using a Student t-test (paired when appropriate) and their correlation measured using a Pearson product-moment correlation coefficient *r*. Regurgitation grades were compared using a Wilcoxon signed rank test. Parameters are

reported as mean ± standard deviation. Right atrial and ventricular cerclage success were compared using a Fisher exact test. A p value < 0.05 is considered significant.

Results

Cerclage creation

We identified two suitable cerclage guidewire trajectories [Figure 1A, B]. A “simple,” or right ventricular, cerclage traverses a short distance of myocardium into the nearby right ventricular outflow tract. The wire re-enters the right atrium along the septal tricuspid valve commissure. A “right atrial” cerclage trajectory extends from the septal vein further inside the basal septal myocardium into the right atrium near the coronary sinus ostium. Upon reentry the guidewire moves freely, as it does after successful recanalization of arterial occlusion. To avoid trabecular entrapment, the guidewire is directed into the pulmonary artery, ensnared, externalized, and replaced with a suture. Graded cerclage tension can be applied to both ends of the cerclage suture, interactively during MRI until further tension did not further abate regurgitation. Finally a fixation device secures the tension near the origin of the coronary sinus.

Technical success and complications

Figure 1-C–E illustrate XFM-guided trajectory planning for myocardial guidewire traversal.

The first consecutive 12 cerclage attempts failed. In the next 13 consecutive technical development experiments, cerclage was successful in 8 (62%) naïve swine. Of these, one suffered coronary sinus thrombosis attributed to prolonged guiding catheter manipulation, another suffered tricuspid chordal transection by an entrapped cerclage guidewire, and another suffered intraventricular conduction delay.

In the third phase in 16 consecutive swine with ischemic cardiomyopathy, cerclage was successful in 14 (88%). Both failures were nonfatal exit (perforation) into the pericardium, once from the right ventricular free wall, and another from the left ventricular septum. These are attributed to inadequate use of imaging guidance to distinguish the septum and free wall. There were two major complications, including one pericardial tamponade during jugular vein access, and high degree atrioventricular block after right atrial cerclage. One animal developed reversible tricuspid valve regurgitation after right ventricular cerclage tension entrapped a variant septal tricuspid valve leaflet.

Combining naïve and myopathic animals, right ventricular cerclage succeeded in 15/16 animals (94%) compared with right atrial cerclage (7/10 animals, 70% success, p=0.26). Right ventricular cerclage required less fluoroscopy (55±20 minutes versus 144±84 minutes, p=0.02).

Necropsy examination confirmed the predicted guidewire trajectory for right ventricular [Figure 1-G] and right atrial [Figure 1-H] cerclage. In right ventricular cerclage, the suture traversed a 28 ± 4.8mm intraseptal path measured from the epicardium including approximately 15mm of septal vein, passed near tricuspid chordae and reentered the right atrium along the septal tricuspid commissure.

A minority of animals had unsuitable coronary venous anatomy by coronary venography. A great cardiac vein was not contiguous with the coronary sinus in 4 of 45 animals, which were excluded from analysis. One animal had an absent basal septal perforating vein but underwent successful right ventricular cerclage using an enhanced-stiffness guidewire (a transected *Confianza*).

Protection of entrapped coronary arteries

Major circumflex coronary artery branches were entrapped by the cerclage suture in all animals. Cerclage with 400g tension induced subtotal angiographic occlusion [Figure 2-E] and halved resting distal coronary pressure without a protection device in place [Figure 2-G].

With the coronary artery protection device deployed, cerclage tension caused no angiographic stenosis [Figure 2-F] or relative reduction in distal coronary pressure, even at supra-therapeutic (800g) tension that impaired trans-mitral filling and lowered systemic blood pressure [Figure 2-H]. The protection device remained in deployed position in all animals assessed at necropsy, and remained effective in one animal survived for six weeks.

Impact of cerclage on mitral annulus and left ventricle geometry

Graded tension progressively reduced the septal-lateral dimension of the mitral annulus but not significantly the commissural width [Figure 3-A and Table 1]. Compared with baseline, 600g of tension reduced septal-lateral dimension approximately 20% in both systole and diastole. The septal-lateral diameter fell in linear proportion to cerclage diameter as tension was applied [Figure 3-B), r^2=0.54.

Ventricular volumes declined non-significantly when tension was applied [Table 1], and left ventricular ejection fraction fell in these animals with ischemic cardiomyopathy and mitral regurgitation.

Impact of cerclage on myocardial function

Progressive tension did not reduce conductance-catheter based measures of global myocardial performance. End-systolic elastance (E_{es}), the slope of end-systolic pressure-volume relationship as preload changes, was 2.2 ± 1.3 mm Hg/mL at baseline and 2.6 ± 1.5 mm Hg/mL during tension, p<0.01 [Figure 4].

MRI regional wall motion appeared unaffected by cerclage (wall motion score index 1.54± 0.12 before *versus* 1.56± 0.16 after cerclage, p=0.76). No new late gadolinium enhancement was evident to suggest cerclage-induced myocardial infarction.

One animal of 16 with ischemic cardiomyopathy suffered high degree atrioventricular block associated with pericardial tamponade. In the others, cerclage tension induced no ECG depolarization or repolarization abnormalities.

Mitral valve regurgitation

Two thirds of animals surviving with ischemic cardiomyopathy (ejection fraction 39.2 ± 7.6) developed significant mitral regurgitation (n=10). Successful cerclage reduced mitral valve regurgitation. Figure 5 and video 1 depict a representative animal with severe ischemic cardiomyopathy before and after application of cerclage tension. Black jets of dephased spins are seen regurgitating from the left ventricle (arrows). After applying 400g of cerclage tension (panel B) the septal lateral annular dimension (between arrowheads 1 and 2) is reduced, as is the cerclage diameter (between arrowheads 3 and 4). Regurgitant jets are no longer evident. Discordant cerclage and annular planes are evident and the coronary sinus (arrowhead 4) does not overlap the posterior annulus (arrowhead 2).

Velocity encoded MRI was available for five animals. In these, the regurgitant fraction was reduced from 22.8 ± 12.7% to 7.2 ± 4.4% (p=0.04) when cerclage tension was applied [Figure 6 and Table 2]. Results are similar using radiocontrast ventriculography (n=10).

In preliminary experiments, three animals were survived for three weeks or more after cerclage without recurrent mitral regurgitation or evident myocardial erosion.

Figure 5-C–D and video 2 show simultaneous tagged and color-flow MRI in an animal with mitral regurgitation that is reduced by cerclage tension. Posterobasal myocardial thinning, late enhancement, and severe hypokinesis also are evident as expected in this ischemic cardiomyopathy model.

Mitral valve tenting area, a measure of annular dilation and subvalvular traction, was reduced after application of cerclage tension [Table 2]. The degree of tenting was reduced in proportion to the reduction in cerclage diameter [Figure 3-C]. By virtue of reducing septal lateral distance, the posterior displacement of the line of coaptation was reduced by cerclage.

Cerclage tension did not significantly change two-dimensional measures of mitral leaflet curvature and angulation with regard to the annulus (Table 3), which reflect leaflet traction.

Discordant Annular and Cerclage Planes

Variable coronary sinus anatomy contributes to discordant cerclage and mitral annular planes [Figure 1-F]. In our pig model, the average maximum distance of the coronary sinus to the mitral annulus was 6.6 ± 2.0 mm and the angle of the two planes was 21.8 ± 6.4°. These did not vary significantly throughout the cardiac cycle or during application of tension.

Because the posterior coronary sinus may pass along the atrial aspect of the mitral valve annulus, the vector difference of these discordant planes contributes an apical displacement force to the cerclage annuloplasty.

Mitral annular geometry and motion

Cerclage induced conformational changes in the mitral valve annulus (Table 3). Mitral annular area (measured as a three-dimensional surface) fell with application of tension. Mitral annular geometry varied throughout the cardiac cycle [Figure 7]. This cyclical annular contraction is preserved despite application of cerclage tension, which nevertheless reduced circumference and septal-lateral width. Annular height to commissure width ratio is increased by cerclage, which alters the annular saddle morphology. Tension acted to displace the posterior annulus caudally, towards the posterior papillary muscle [Figure 7-E–F, videos 3–4].

Reciprocal constraint of mitral annulus and left ventricular outflow tract

Cerclage annuloplasty encircles both the mitral annulus and the left ventricular outflow tract [Figure 8] and Table 4. We observed reciprocal constraint of these two structures during the cardiac cycle when cerclage tension was applied. Whereas the cerclage diameter remains fixed throughout the cardiac cycle, the left ventricular outflow tract diameter enlarges during systole and contracts during diastole. Conversely, the constrained septal-lateral dimension of the mitral annulus is reduced by the left ventricular outflow tract during systole but not constrained during diastole. There was no gradient induced across the left ventricular outflow tract using conventional fluid-filled catheters, nor was aortic regurgitation induced.

Anatomic suitability of humans

We reviewed pressurized coronary venous angiograms in 10 patients with congestive heart failure undergoing cardiac resynchronization therapy. Eight had evident proximal septal coronary veins arising from the great cardiac vein that appear suitable for cerclage [Figure 9]. The other two had inadequate angulation to view septal perforator veins.

We also reviewed 29 sequential CT angiograms in a coronary teaching file. The mean age was 53.2 ± 12.3 years, 79% were male. Of these, 24 (83%) had proximal septal perforator veins that appear suitable for cerclage.

Discussion

We have developed a novel procedure for catheter-based mitral cerclage annuloplasty. We have shown circumferential tension can be introduced near the mitral annulus plane via basal septal perforator veins in swine; that attainable tension reduces annular circumference and septal-lateral diameter; that annuloplasty does not appear to alter measures of global myocardial performance; that a simple device protects entrapped coronary artery branches even during supra-therapeutic annuloplasty tension; and in a preliminary review that humans appear to have comparable coronary septal perforator vein anatomy.

We have also shown that cerclage annuloplasty immediately attenuates functional mitral valve regurgitation in a clinically-relevant animal model of ischemic cardiomyopathy characterized by left ventricular dysfunction, mitral annular dilation and posterior papillary muscle traction. Qualitative and quantitative measures of mitral regurgitation are reduced immediately after cerclage. Magnetic resonance imaging has provided insight into the mechanism of cerclage action. First, flexible cerclage reduces annular size while preserving annular motion. Second, in this model, the cerclage suture folds the annulus and displaces the posterior annulus caudally, apparently to accommodate posterior papillary traction. Third, cerclage introduces reciprocal constraint to the left ventricular outflow tract and mitral annulus such that systolic ejection enhances anterior mitral leaflet coaptation.

Anatomic and geometric factors appear to limit innovative approaches to transcatheter coronary-sinus-based annuloplasty reported previously. First, the coronary sinus often courses along the left atrial wall far from the mitral annular plane. Second, the coronary sinus usually entraps underlying major coronary artery branches, so annular compression can induce myocardial ischemia. Third, non-circumferential coronary sinus annuloplasty devices may limit annular shortening to only a small arc of annular circumference.

Cerclage annuloplasty addresses these shortcomings. The crossing planes of the mitral annulus and the cerclage trajectory [Figure 1-F] permit effective reduction of the septal-lateral dimension even though the coronary sinus plane does not parallel the annulus. Our protection device averts coronary artery compression, and may have value in other coronary-sinus based annuloplasty approaches. Circumferential cerclage constrains the annulus including the fibrous trigones, unlike other coronary sinus-based devices.

Annuloplasty

Functional mitral regurgitation is a manifestation of severe myocardial dysfunction(1) associated with worse symptoms and prognosis. Global and regional myocardial dysfunction and remodeling contribute to functional mitral regurgitation through annular dilation, traction by displaced and elongated chordal-papillary apparatus (usually posterior), regional left ventricular dyssynchrony, and deleterious compensatory loading conditions. Non-surgical treatment may include cardiac resynchronization therapy, beta adrenergic blockade, and angiotensin converting enzyme inhibitors. Surgical repair for organic mitral regurgitation has been extended to patients with cardiomyopathy and normal mitral leaflets. Bolling and colleagues(37) advocate “undersized” annuloplasty. Additional surgical options include papillary-chordal repair, reinforcement, relocation, ligation, or bowtie constraint of the leaflets (38,39). Myocardial reduction procedures or constraining devices also are under development (2,4).

The choice of rigid or flexible annuloplasty devices remains controversial. Normal hearts exhibit cyclic contraction of the mitral valve annulus which may enhance leaflet coaptation(40,41). Preserved annular contraction is associated with a smaller effective regurgitant orifice (32,40). Rigid annuloplasty rings impede mitral annular contraction and tilting. Partial bands, flexible rings, or open suture annuloplasty(42) preserve annular dynamics and have been advocated as a more “physiologic” annuloplasty associated with lower trans-valvular gradients. However, flexible annuloplasty rings may contribute to late recurrence of mitral regurgitation compared with rigid rings (43).

In some reports(31) rigid annuloplasty exacerbates leaflet tethering by displacing the posterior annulus further away from the papillary muscles. Rigid rings have been developed to compensate for the P2–P3 leaflet tethering by enforcing an apical “dip” in the posterior annulus(44) much like we observe after cerclage. The saddle morphology of the normal mitral annulus may confer a mechanical advantage of reduced leaflet stress (45,46) that may be reduced by annular flattening in functional mitral regurgitation(33,47). Like flexible annuloplasty and suture annuloplasty(42), cerclage preserves annular dynamics and restores annular height. Like newer rigid annuloplasty devices, cerclage serendipitously redistributes the posterior segment to accommodate apical tethering. However, cerclage appears to induce a more complex shape than the natural annular hyperbolic paraboloid.

Our measures of leaflet configuration and leaflet traction are similar to those reported in patients undergoing surgical repair of ischemic mitral valve regurgitation(31). In that report, persistent posterior leaflet traction (wide α2) corresponded with failed surgical repair. After cerclage, we found the angular relation of the posterior leaflet with the annulus to be comparably narrow. In our experiments, the length of the coaptation line increased nonsignificantly.

Initially we were concerned that entrapment of the left ventricular outflow tract, inevitable with a trans-septal venous cerclage trajectory, might induce dynamic left ventricular outflow tract obstruction. On the contrary, we found reciprocal enlargement of the entrained left ventricular outflow tract and reduction of septal-lateral distance by cerclage during systole. This interaction improved mitral leaflet coaptation during systole and relaxed the mitral orifice during diastolic filling. Similar aorto-mitral interaction has been reported in healthy sheep(48), but was not evident in our experiments until cerclage tension was applied.

Mild-moderate mitral regurgitation is hard to measure, especially using magnetic resonance imaging (49), which for clinically relevant examinations tends to have inferior time resolution and leaflet visualization. The severity of mitral regurgitation varies with loading conditions(50), further confounding measurement. Echocardiography in swine has proven unsuitable in our laboratories because of inadequate imaging windows. We therefore used velocity-encoded MRI with slice-tracking to measure through-plane regurgitation across the moving mitral valve plane(51).

Imaging Guidance

Because neither conventional X-ray nor ultrasound alone satisfactorily depicts myocardial structures and devices during cerclage, we used fusion image guidance. We superimposed MRI-derived roadmaps onto live X-ray, using a system that compensates automatically for changes in table position or gantry orientation(28).

Failure modes and limitations

This is an early experience with a new procedure using largely off-the-shelf catheter tools. We considered several potential failure modes.

Cerclage suture applies non-physiological centripetal force to multiple structures and may risk chronic erosion. Erosion does not appear limiting after other tangential myocardial sutures including “Fontan” endoventricular pursestring and Paneth-Burr mitral annuloplasty. In general erosion is related to suture tension and tissue friability and inversely related to suture diameter and time to scar formation. To mitigate the local force and erosion risk, we selected a cerclage suture significantly larger (0.8mm versus 0.3mm) than 2-0 suture commonly used in myocardial applications with- or without pledgets. No erosion was evident in a small number of animals survived after cerclage. These considerations must be further tested in survival experiments. Guidewire-based cerclage traversal of the interventricular septum is a “blunt dissection” that has not evidently entered or interrupted visible septal perforator arteries to date. Right ventricular cerclage reenters the coronary sinus ostium across the tricuspid commissure and may encroach on the Koch triangle but generally not its apex, where the compact atrioventricular nodal is located.

Right ventricular cerclage requires care to avoid tricuspid valve injury. Chordal entrapment can be avoided by deflecting the guidewire immediately into the pulmonary artery upon right ventricular reentry. Leaflet entrapment was observed in one animal with variant septal leaflet anatomy and ventricular septal defect. There was no leaflet entrapment when cerclage suture crossed “normal” septal tricuspid commissures, which should be identifiable on cardiac CT or MRI. There is precedent for chronic implantation of pacemaker and defibrillator leads across the tricuspid valve, albeit not under intentional tension. Tricuspid valve function does not appear affected by right ventricular cerclage (data not shown) with tension across the septal tricuspid commissure.

By contrast, right atrial cerclage avoids the tricuspid valve entirely. Right atrial cerclage is more technically demanding, and was associated with conduction block in one animal. Further data are necessary to understand the interaction of right atrial cerclage and normal and pathologic conduction tissue(52).

While cerclage does not appear possible if the great cardiac vein is not connected to the coronary sinus, in one case we were able to complete cerclage even without an evident basal septal perforator vein. Incorrect guidewire traversal of, for example, a right ventricular free wall, likely can be avoided with procedure experience and enhanced image guidance.

We have shown that compression of entrapped circumflex coronary artery branches can be averted by implanting a simple protection device along the cerclage suture. We are developing a more sophisticated low-profile tension-fixation device.

We are not able to generate severe functional mitral regurgitation in our porcine model of ischemic cardiomyopathy. Regurgitation severity may have been reduced by our use of isoflurane anesthesia(53).

The durability of our short term findings is not known. The coronary sinus is typically connected to the mitral annulus by non-fibrous atrial myocardium(54). Chronic remodeling of this sino-annular tissue might contribute to late failure of cerclage annuloplasty. Conversely, intertrigonal remodeling may be less likely after circumferential cerclage, compared with flexible annuloplasty bands, which are attached to the trigones only.

Mitral valve repair may not benefit patients with cardiomyopathy(55–58), even though the perioperative mortality may be low in experienced hands. Surgical repair is usually performed with concomitant myocardial revascularization. Whether primary mitral valve repair improves symptoms or outcome remains to be tested(59). Moreover, we cannot predict where cerclage annuloplasty, if it proves technically successful in humans, would fit into a therapeutic armamentarium against heart failure with mitral regurgitation.

Conceivably it could be combined with effective pharmacologic and cardiac resynchronization treatments, and it would not likely interfere with subsequent surgical valve or myocardial procedures. Cerclage might be used as an adjunct to catheter-based Alfieri-type bowtie repair which, without annuloplasty, may generate excessive stitch and leaflet tension(60). Early repair of ischemic mitral regurgitation may reverse deleterious remodeling in some animal models(61) but not others(62).

Conclusion

Transcatheter cerclage annuloplasty delivers circumferential annular tension around the mitral annulus and left ventricular outflow tract. Cerclage shrinks the mitral annulus and immediately abates mitral regurgitation in an animal model of chronic ischemic cardiomyopathy. MRI of annular configuration and dynamics suggests cerclage acts by more than reducing annular size. Cyclical annular motion is preserved and height restored. The posterior annulus is displaced toward the posterior papillary apparatus. Reciprocal constraint of the mitral annulus and the left ventricular outflow tract appears to contribute to mitral leaflet coaptation. Entrapped coronary arteries can be protected from extrinsic compression using a simple arch-like device implanted over the cerclage suture. Other potential failure modes appear non-limiting. A preliminary review of human venograms and CT angiograms suggest a majority have suitable venous anatomy. Further experiments will test the longer-term impact of this approach.

Supplementary Material

Refer to Web version on PubMed Central for supplementary material.

Acknowledgments

We are grateful to Katherine Lucas and Joni Taylor for animal experiments, to David Bush and Edward Shapiro of Johns Hopkins Bayview for anonymized CT images, to Michael Lee and Raj Makkar of Cedars-Sinai for anonymized coronary venograms, and to Lydia Kibiuk of NIH Medical Arts for illustrations. Siemens Corporate Research supported and Christine Lorenz mentored two graduate students (MS and Akin Yucetas) who contributed to MRI-X-ray registration and investigational velocity-encoded MRI techniques.

Abbreviations

CT	Computed tomography
MRI	Magnetic resonance imaging
SSFP	Steady state free precession MRI
TE	MRI echo time
TR	MRI repetition time
XFM	X-ray fused with MRI

References

1. Levine RA, Schwammenthal E. Ischemic mitral regurgitation on the threshold of a solution: from paradoxes to unifying concepts. Circulation 2005;112:745–58. [PubMed: 16061756]
2. Fedak PW, McCarthy PM, Bonow RO. Evolving concepts and technologies in mitral valve repair. Circulation 2008;117:963–74. [PubMed: 18285577]
3. Chen FY, Adams DH, Aranki SF, et al. Mitral valve repair in cardiomyopathy. Circulation 1998;98:II124–7. [PubMed: 9852893]

4. Acker MA, Bolling S, Shemin R, et al. Mitral valve surgery in heart failure: insights from the Acorn Clinical Trial. J Thorac Cardiovasc Surg 2006;132:568–77. 577, e1–4. [PubMed: 16935112]
5. Liddicoat JR, Mac Neill BD, Gillinov AM, et al. Percutaneous mitral valve repair: a feasibility study in an ovine model of acute ischemic mitral regurgitation. Catheter Cardiovasc Interv 2003;60:410–6. [PubMed: 14571496]
6. Kaye DM, Byrne M, Alferness C, Power J. Feasibility and short-term efficacy of percutaneous mitral annular reduction for the therapy of heart failure-induced mitral regurgitation. Circulation 2003;108:1795–7. [PubMed: 14530194]
7. Maniu CV, Patel JB, Reuter DG, et al. Acute and chronic reduction of functional mitral regurgitation in experimental heart failure by percutaneous mitral annuloplasty. J Am Coll Cardiol 2004;44:1652–61. [PubMed: 15489099]
8. Daimon M, Shiota T, Gillinov AM, et al. Percutaneous mitral valve repair for chronic ischemic mitral regurgitation: a real-time three-dimensional echocardiographic study in an ovine model. Circulation 2005;111:2183–9. [PubMed: 15851597]
9. Duffy SJ, Federman J, Farrington C, Reuter DG, Richardson M, Kaye DM. Feasibility and short-term efficacy of percutaneous mitral annular reduction for the therapy of functional mitral regurgitation in patients with heart failure. Catheter Cardiovasc Interv 2006;68:205–10. [PubMed: 16817176]
10. Webb JG, Harnek J, Munt BI, et al. Percutaneous transvenous mitral annuloplasty: initial human experience with device implantation in the coronary sinus. Circulation 2006;113:851–5. [PubMed: 16461812]
11. Dubreuil O, Basmadjian A, Ducharme A, et al. Percutaneous mitral valve annuloplasty for ischemic mitral regurgitation: first in man experience with a temporary implant. Catheter Cardiovasc Interv 2007;69:1053–61. [PubMed: 17525965]
12. Rogers JH, Macoviak JA, Rahdert DA, Takeda PA, Palacios IF, Low RI. Percutaneous septal sinus shortening: a novel procedure for the treatment of functional mitral regurgitation. Circulation 2006;113:2329–34. [PubMed: 16682615]
13. Palacios IF, Condado JA, Brandi S, et al. Safety and feasibility of acute percutaneous septal sinus shortening: First-in-human experience. Catheter Cardiovasc Interv 2007;69:513–8. [PubMed: 17323357]
14. Pedersen WR, Block P, Leon M, et al. iCoapsys mitral valve repair system: Percutaneous implantation in an animal model. Catheter Cardiovasc Interv 2008;72:125–31. [PubMed: 18561162]
15. Hlavka, EJ.; Podmore, JL.; Spence, PA., inventors. Method and apparatus for catheter-based annuloplasty using local plications. US patent. 6718985. 2004 Apr 13. Mitralign, assignee
16. Hung J, Solis J, Guerrero JL, et al. A novel approach for reducing ischemic mitral regurgitation by injection of a polymer to reverse remodel and reposition displaced papillary muscles. Circulation 2008;118:S263–9. [PubMed: 18824765]
17. St Goar FG, Fann JI, Komtebedde J, et al. Endovascular edge-to-edge mitral valve repair: short-term results in a porcine model. Circulation 2003;108:1990–3. [PubMed: 14530193]
18. Fann JI, St Goar FG, Komtebedde J, et al. Beating heart catheter-based edge-to-edge mitral valve procedure in a porcine model: efficacy and healing response. Circulation 2004;110:988–93. [PubMed: 15302782]
19. Feldman T, Wasserman HS, Herrmann HC, et al. Percutaneous mitral valve repair using the edge-to-edge technique: six-month results of the EVEREST Phase I Clinical Trial. J Am Coll Cardiol 2005;46:2134–40. [PubMed: 16325053]
20. Naqvi TZ, Buchbinder M, Zarbatany D, et al. Beating-heart percutaneous mitral valve repair using a transcatheter endovascular suturing device in an animal model. Catheter Cardiovasc Interv 2007;69:525–31. [PubMed: 17323355]
21. Choure AJ, Garcia MJ, Hesse B, et al. In vivo analysis of the anatomical relationship of coronary sinus to mitral annulus and left circumflex coronary artery using cardiac multidetector computed tomography: implications for percutaneous coronary sinus mitral annuloplasty. J Am Coll Cardiol 2006;48:1938–45. [PubMed: 17112981]

22. Maselli D, Guarracino F, Chiaramonti F, Mangia F, Borelli G, Minzioni G. Percutaneous mitral annuloplasty: an anatomic study of human coronary sinus and its relation with mitral valve annulus and coronary arteries. Circulation 2006;114:377–80. [PubMed: 16864726]
23. Tops LF, Van de Veire NR, Schuijf JD, et al. Noninvasive evaluation of coronary sinus anatomy and its relation to the mitral valve annulus: implications for percutaneous mitral annuloplasty. Circulation 2007;115:1426–32. [PubMed: 17353434]
24. Tops LF, Van de Veire NR, Schuijf JD, et al. Noninvasive evaluation of coronary sinus anatomy and Its relation to the mitral valve annulus. Implications for percutaneous mitral annuloplasty. Circulation. 2007
25. Croft LR, Jimenez JH, Gorman RC, Gorman JH 3rd, Yoganathan AP. Efficacy of the edge-to-edge repair in the setting of a dilated ventricle: an in vitro study. Ann Thorac Surg 2007;84:1578–84. [PubMed: 17954065]
26. Glover RP, Davila JC. Surgical treatment of mitral insufficiency by total circumferential purse-string suture of the mitral ring. Circulation 1957;15:661–81. [PubMed: 13427121]
27. Swindle MM, Horneffer PJ, Gardner TJ, et al. Anatomic and anesthetic considerations in experimental cardiopulmonary surgery in swine. Lab Anim Sci 1986;36:357–61. [PubMed: 3534438]
28. de Silva R, Gutierrez LF, Raval AN, McVeigh ER, Ozturk C, Lederman RJ. X-ray fused with magnetic resonance imaging (XFM) to target endomyocardial injections: validation in a swine model of myocardial infarction. Circulation 2006;114:2342–50. [PubMed: 17101858]
29. Gutiérrez LF, Silva R, Ozturk C, et al. Technology preview: X-ray fused with magnetic resonance during invasive cardiovascular procedures. Catheter Cardiovasc Interv 2007;70:773–82. [PubMed: 18022851]
30. Schiller NB, Shah PM, Crawford M, et al. Recommendations for quantitation of the left ventricle by two-dimensional echocardiography. American Society of Echocardiography Committee on Standards, Subcommittee on Quantitation of Two-Dimensional Echocardiograms. J Am Soc Echocardiogr 1989;2:358–67. [PubMed: 2698218]
31. Zhu F, Otsuji Y, Yotsumoto G, et al. Mechanism of persistent ischemic mitral regurgitation after annuloplasty: importance of augmented posterior mitral leaflet tethering. Circulation 2005;112:I396–401. [PubMed: 16159853]
32. Yiu SF, Enriquez-Sarano M, Tribouilloy C, Seward JB, Tajik AJ. Determinants of the degree of functional mitral regurgitation in patients with systolic left ventricular dysfunction: A quantitative clinical study. Circulation 2000;102:1400–6. [PubMed: 10993859]
33. Kaji S, Nasu M, Yamamuro A, et al. Annular geometry in patients with chronic ischemic mitral regurgitation: three-dimensional magnetic resonance imaging study. Circulation 2005;112:I409–14. [PubMed: 16159855]
34. Dujardin KS, Enriquez-Sarano M, Bailey KR, Nishimura RA, Seward JB, Tajik AJ. Grading of mitral regurgitation by quantitative Doppler echocardiography: calibration by left ventricular angiography in routine clinical practice. Circulation 1997;96:3409–15. [PubMed: 9396435]
35. Sampath S, Kim JH, Lederman RJ, McVeigh ER. Simultaneous imaging of myocardial motion and chamber blood flow with SPAMM n' EGGS (spatial modulation of magnetization with encoded gradients for gauging speed). Journal of Magnetic Resonance Imaging 2008;27:809–817. [PubMed: 18383258]
36. Steendijk P, Staal E, Jukema JW, Baan J. Hypertonic saline method accurately determines parallel conductance for dual-field conductance catheter. Am J Physiol Heart Circ Physiol 2001;281:H755–63. [PubMed: 11454580]
37. Bolling SF, Pagani FD, Deeb GM, Bach DS. Intermediate-term outcome of mitral reconstruction in cardiomyopathy. J Thorac Cardiovasc Surg 1998;115:381–6. [PubMed: 9475533]
38. Savage, EB.; Bolling, SF. Atlas of mitral valve repair. Philadelphia: Lippincott Williams & Wilkins; 2006.
39. Borger MA, Alam A, Murphy PM, Doenst T, David TE. Chronic ischemic mitral regurgitation: repair, replace or rethink? Ann Thorac Surg 2006;81:1153–61. [PubMed: 16488757]

40. Tsakiris AG, Von Bernuth G, Rastelli GC, Bourgeois MJ, Titus JL, Wood EH. Size and motion of the mitral valve annulus in anesthetized intact dogs. J Appl Physiol 1971;30:611–8. [PubMed: 5576071]
41. Dent JM, Spotnitz WD, Nolan SP, Jayaweera AR, Glasheen WP, Kaul S. Mechanism of mitral leaflet excursion. Am J Physiol 1995;269:H2100–8. [PubMed: 8594922]
42. Tibayan FA, Rodriguez F, Liang D, Daughters GT, Ingels NB Jr, Miller DC. Paneth suture annuloplasty abolishes acute ischemic mitral regurgitation but preserves annular and leaflet dynamics. Circulation 2003;108(Suppl 1):II128–33. [PubMed: 12970221]
43. Spoor MT, Geltz A, Bolling SF. Flexible versus nonflexible mitral valve rings for congestive heart failure: differential durability of repair. Circulation 2006;114:I67–71. [PubMed: 16820648]
44. Daimon M, Fukuda S, Adams DH, et al. Mitral valve repair with Carpentier-McCarthy-Adams IMR ETlogix annuloplasty ring for ischemic mitral regurgitation: early echocardiographic results from a multi-center study. Circulation 2006;114:I588–93. [PubMed: 16820643]
45. Salgo IS, Gorman JH 3rd, Gorman RC, et al. Effect of annular shape on leaflet curvature in reducing mitral leaflet stress. Circulation 2002;106:711–7. [PubMed: 12163432]
46. Jimenez JH, Liou SW, Padala M, et al. A saddle-shaped annulus reduces systolic strain on the central region of the mitral valve anterior leaflet. J Thorac Cardiovasc Surg 2007;134:1562–8. [PubMed: 18023684]
47. Tibayan FA, Rodriguez F, Langer F, et al. Annular remodeling in chronic ischemic mitral regurgitation: ring selection implications. Ann Thorac Surg 2003;76:1549–54. discussion 1554–5. [PubMed: 14602284]
48. Timek TA, Green GR, Tibayan FA, et al. Aorto-mitral annular dynamics. Ann Thorac Surg 2003;76:1944–50. [PubMed: 14667619]
49. Kilner PJ, Gatehouse PD, Firmin DN. Flow measurement by magnetic resonance: a unique asset worth optimising. J Cardiovasc Magn Reson 2007;9:723–8. [PubMed: 17613655]
50. Yoran C, Yellin EL, Becker RM, Gabbay S, Frater RW, Sonnenblick EH. Dynamic aspects of acute mitral regurgitation: effects of ventricular volume, pressure and contractility on the effective regurgitant orifice area. Circulation 1979;60:170–6. [PubMed: 445720]
51. Kozerke S, Schwitter J, Pedersen EM, Boesiger P. Aortic and mitral regurgitation: quantification using moving slice velocity mapping. J Magn Reson Imaging 2001;14:106–12. [PubMed: 11477667]
52. Anderson RH, Ho SY, Becker AE. The surgical anatomy of the conduction tissues. Thorax 1983;38:408–20. [PubMed: 6348996]
53. Grewal KS, Malkowski MJ, Piracha AR, et al. Effect of general anesthesia on the severity of mitral regurgitation by transesophageal echocardiography. Am J Cardiol 2000;85:199–203. [PubMed: 10955377]
54. Hueb AC, Jatene FB, Moreira LF, Pomerantzeff PM, Kallas E, de Oliveira SA. Ventricular remodeling and mitral valve modifications in dilated cardiomyopathy: new insights from anatomic study. J Thorac Cardiovasc Surg 2002;124:1216–24. [PubMed: 12447190]
55. Gorman JH 3rd, Gorman RC. Mitral valve surgery for heart failure: a failed innovation? Semin Thorac Cardiovasc Surg 2006;18:135–8. [PubMed: 17157234]
56. Wu AH, Aaronson KD, Bolling SF, Pagani FD, Welch K, Koelling TM. Impact of mitral valve annuloplasty on mortality risk in patients with mitral regurgitation and left ventricular systolic dysfunction. J Am Coll Cardiol 2005;45:381–7. [PubMed: 15680716]
57. Mihaljevic T, Lam BK, Rajeswaran J, et al. Impact of mitral valve annuloplasty combined with revascularization in patients with functional ischemic mitral regurgitation. J Am Coll Cardiol 2007;49:2191–201. [PubMed: 17543639]
58. Braun J, van de Veire NR, Klautz RJ, et al. Restrictive mitral annuloplasty cures ischemic mitral regurgitation and heart failure. Ann Thorac Surg 2008;85:430–6. [PubMed: 18222238]
59. Adams DH, Anyanwu A. Pitfalls and limitations in measuring and interpreting the outcomes of mitral valve repair. J Thorac Cardiovasc Surg 2006;131:523–9. [PubMed: 16515900]
60. Timek TA, Nielsen SL, Lai DT, et al. Effect of chronotropy and inotropy on stitch tension in the edge-to-edge mitral repair. Circulation 2007;116:I276–81. [PubMed: 17846317]

61. Beeri R, Yosefy C, Guerrero JL, et al. Early repair of moderate ischemic mitral regurgitation reverses left ventricular remodeling: a functional and molecular study. Circulation 2007;116:I288–93. [PubMed: 17846319]

62. Guy TS 4th, Moainie SL, Gorman JH 3rd, et al. Prevention of ischemic mitral regurgitation does not influence the outcome of remodeling after posterolateral myocardial infarction. J Am Coll Cardiol 2004;43:377–83. [PubMed: 15013117]

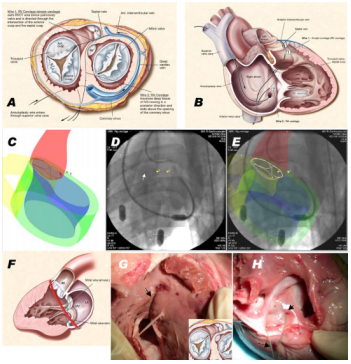

Figure 1.

Schematic, imaging guidance, and necropsy of cerclage annuloplasty. (**A**) shows the mitral annulus from the cardiac apex and (**B**) with free walls of right atrium and ventricle removed. A guidewire through the coronary sinus enters a basal septal perforator vein and traverses a short distance of septal myocardium. Wire 1 follows a right ventricular cerclage trajectory into the right ventricular outflow tract, and wire 2 a longer trajectory to reenter the right atrium directly. The guidewire is replaced with a suture and tension applied to both ends and fixed near the coronary sinus ostium. (**C–E**) shows XFM procedure guidance. MRI-derived contours include LV and RV endocardium (blue and yellow), LV epicardium (green), and aortic root (red). (**D**) shows live X-ray fluoroscopy and (**E**) the corresponding XFM display. The guidewire tip (white arrow) crosses septal myocardium and reenters the right ventricle. Registration is maintained even when the table or gantry move. (**F**) shows the discordant planes of the mitral annulus (blue) and cerclage annuloplasty (red). Necropsy findings are shown immediately after right ventricular (**G**) and right atrial (**H**) cerclage with the RV free wall removed. In (**G**) the suture (arrow) emerges from the septum and returns to the right atrium across a tricuspid commissure. In (**H**) a suture emerges (arrow) near the cavo-tricuspid isthmus, alongside the coronary sinus end of the same suture (dotted arrow). Panels A,B,F courtesy of Lydia Kibiuk, NIH Medical Arts.

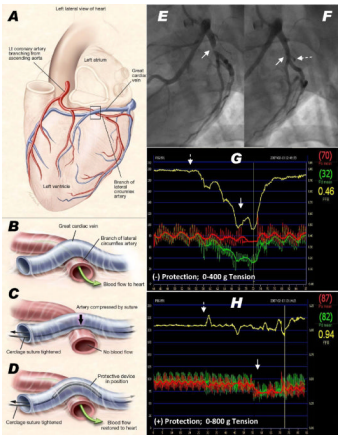

Figure 2.

Coronary artery entrapment and protection. (**A,B)** A typical great cardiac vein configuration passing outside a circumflex artery branch. (**C**) Cerclage would compress the underlying artery. (**D)** A protection device along the cerclage suture redistributes compressive forces away from coronary artery. (**E–H**) circumflex coronary artery pressure during cerclage tension without (**E,G**) and with (**F,H**) a protection device in place. (**E**) Angiographic stenosis (arrow) induced by cerclage and (**F**) the same segment during cerclage tension with a protection device (dashed arrow) in place. (**G,H**) Distal coronary artery pressure (Pd, depicted in green, axis on left, mm), the aortic pressure (Pa) in red, and their ratio in yellow (axis on right, displayed as fractional flow reserve). Without a protection device (**G**), the distal coronary pressure falls by more than half when cerclage tension (400g) is applied. (**H**) With the protection device in place, there is no distal pressure drop after cerclage tension is introduced (dotted arrow) until tension is sufficiently high (solid arrow) to impede mitral inflow. Panels A–D courtesy of Lydia Kibiuk, NIH Medical Arts.

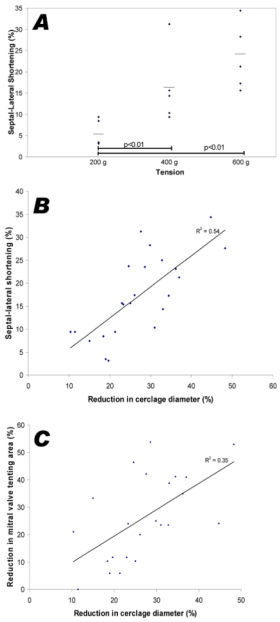

Figure 3.

Effect of graded tension on annular dimensions and leaflet tenting. (**A**) Progressively increased cerclage tension reduces the annular septal-lateral dimension, perpendicular to the line of mitral coaptation. (**B**) With progressive tension, the decline in cerclage diameter is directly related to the decline in septal-lateral dimension. (**C**) Reduced cerclage diameter is directly related to the reduction in mitral valve tenting area, an index of mitral regurgitation.

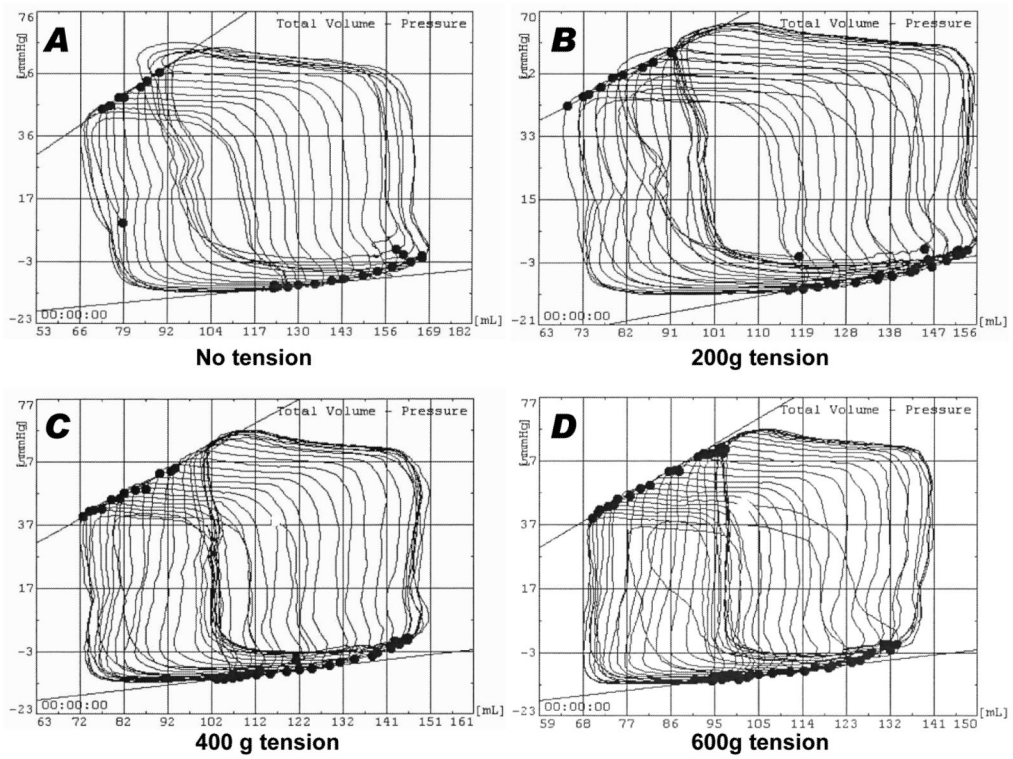

Figure 4.

Representative dynamic pressure-volume loops before (A) and after (B–D) progressive application of cerclage tension in naïve swine. There is no significant change in the end-diastolic (upper slope) and end-systolic (lower slope) pressure-volume relationships as tension is introduced. 600g tension was found to reduce annular circumference sufficiently to impede transmitral inflow. In this animal cerclage does not acutely alter ventricular volumes.

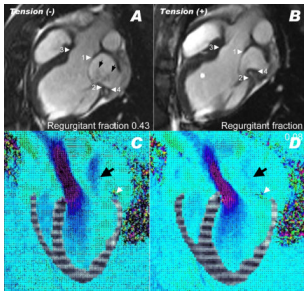

Figure 5.

Mitral regurgitation before (**A,C**) and after (**B,D**) application of cerclage tension. Arrowheads 1 and 2 indicate the anterior and posterior mitral annulus, respectively. Arrowheads 3 and 4 indicate the anterior and posterior course of the cerclage annuloplasty. Arrows indicate the twin jets of mitral regurgitation in this MRI in an animal with a regurgitant fraction of 0.43. After tension is applied, the regurgitant fraction fell to 0.08, and jets are no longer visible. Note the anterior displacement of point 4 and its altered configuration in relation to point 2 (animated in video 1). Note also that regurgitant jets of dephased spins in steady state free precession MRI under-represent mitral regurgitation compared with echocardiography. **(C,D)** show combined motion (tagged) and velocity-encoded MRI during systole before (**C**) and after (**D**) application of cerclage tension in another animal, animated in video 2. Mitral regurgitation is evident as a blue jet in (**C**, black arrow) and nearly extinguished in (**D**). The posterior cerclage wire (black spot indicated by white arrow) is displaced toward the septum when tension is applied. Late gadolinium enhancement and reduced myocardial contraction are evident from prior posterobasal infarction.

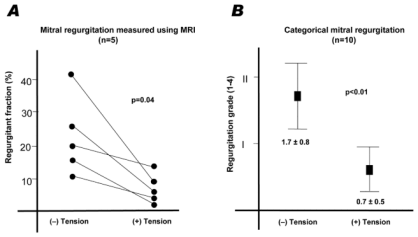

Figure 6.
Quantitative (A) and qualitative (B) measures of mitral regurgitation before and after application of cerclage tension.

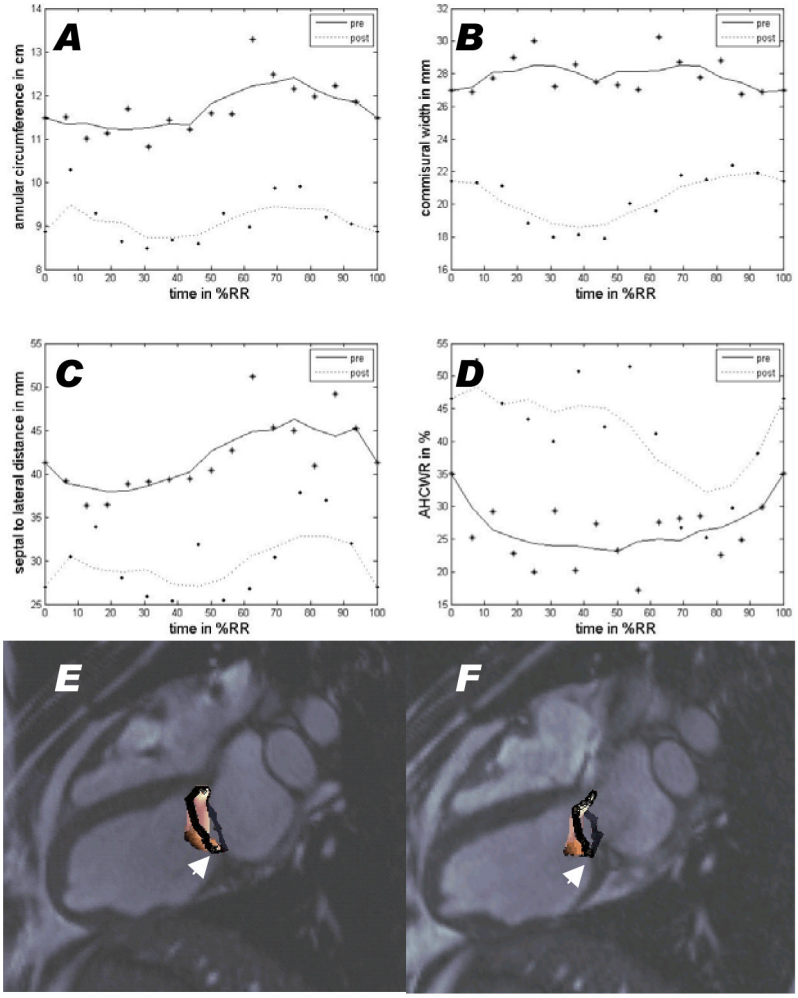

Figure 7.

Dynamics of mitral annulus measurements over time before (solid line) and after (dotted line) cerclage tension is applied. The time scale is normalized for a single cardiac cycle beginning with the QRS gating signal for MRI. Cerclage reduces annular circumference (**A**), commissural width (**B**), and septal-lateral distance (**C**) but increases annular height to commissural width ratio (AHCWR, a measure of annular flattening, **D**). All vary throughout the cardiac cycle and continue to vary despite application of annular tension. **(E–F)** depict the annulus (black) and leaflet (colored) morphology derived from MRI before (**E**) and after (**F**) application of cerclage tension. The posterior annulus (arrow) is displaced caudally toward the posterior papillary muscle when cerclage tension is applied. This is animated in videos 3 and 4.

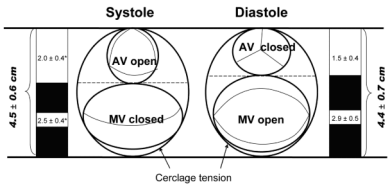

Figure 8.

Reciprocal constraint of the left ventricular outflow tract and mitral annulus after cerclage annuloplasty. The combined diameter of the two structures remains constant throughout the cardiac cycle. During diastole, the anterior mitral leaflet is relatively unconstrained. During systole, the outflow tract enlarges and displaces the anterior mitral valve leaflet posteriorly (* = $p<0.01$ vs diastole). This appears to enhance leaflet coaptation and valve function.

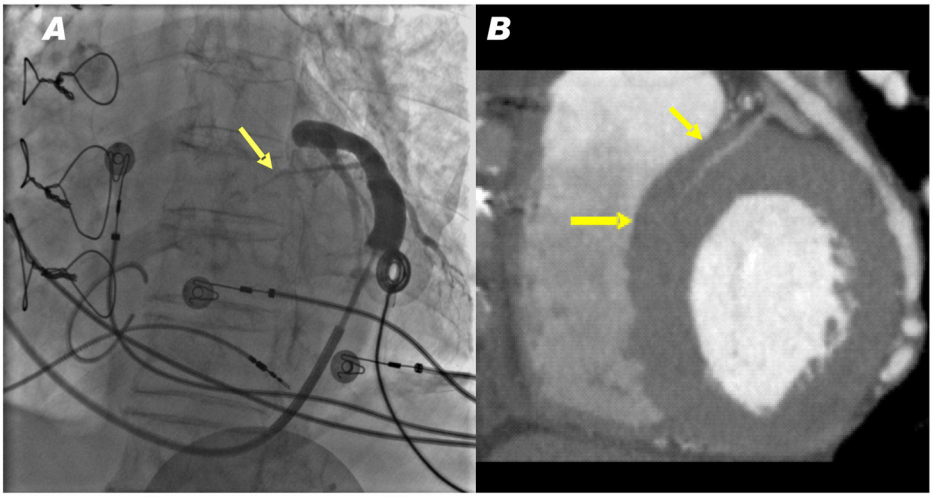

Figure 9.

Representative human venograms. (A) A pressurized venogram in a patient undergoing cardiac resynchronization therapy. A basal septal perforator vein was evident (arrow) in all 8 patients with evaluable angiograms. (B) A CT angiogram showing a basal septal perforator vein (arrows) apparently suitable for cerclage.

Table 1

Impact of cerclage tension on annular and left ventricular dimensions, n=16.

	Baseline	Tension	p value
Mitral annulus			
Septal-lateral annular diameter (cm)			
systole	3.1 ± 0.4	2.5 ± 0.4	<0.001
diastole	3.4 ± 0.6	2.9 ± 0.5	<0.001
Commissural Width (cm)			
systole	2.6 ± 0.3	2.2 ± 0.8	0.41
diastole	2.6 ± 0.4	2.2 ± 1.0	0.28
Cerclage diameter			
Cerclage diameter (cm)	6.2 ± 0.8	4.5 ± 0.8	< 0.001
Left ventricle			
diastolic LVID (cm)	5.4 ± 0.6	5.3 ± 0.6	0.40
systolic LVID (cm)	4.7 ± 0.5	4.6 ± 0.7	0.45
End-systolic volume (ml)	106 ± 43	98 ± 37	0.22
End-diastolic volume (ml)	172 ± 55	158 ± 52	0.09
Ejection fraction	0.39 ± 0.08	0.34 ± 0.04	0.04

Table 2

Measures of mitral valve regurgitation and leaflet function before and after application of cerclage tension (n=10 except for velocity-encoded MRI, n=5).

	Baseline	Tension	*p*
Mitral regurgitation			
Regurgitant fraction by slice-tracking velocity-encoded MRI	22.8 ± 12.7	7.2 ± 4.4	0.04
Categorical mitral regurgitation total (Grade 1–4)	1.7 ± 0.8	0.7 ± 0.5	0.01
Mitral valve coaptation			
Mitral valve tenting area (cm^2)	2.1 ± 0.5	1.5 ± 0.5	0.01
Posterior displacement of line of coaptation (mm)	25.7 ± 4.0	21.2 ± 4.8	0.01
Leaflet coaptation length (mm)	3.0 ± 2.4	4.8 ± 1.6	0.12

Table 3

Leaflet function and annular motion before and after application of cerclage tension in pigs with secondary mitral regurgitation, n=5. Supplemental figure 1 depicts the angles measured.

	Baseline	Tension	*p*
Mitral leaflet configuration and traction			
Anterior leaflet angle with annulus (α1, degrees)	36.6 ± 6.4	34.0 ± 7.9	0.66
Posterior leaflet angle with annulus (α2, degrees)	58.6 ± 21.5	72.2 ± 35.0	0.32
Anterior leaflet curvature (β, degrees)	145 ± 11	150 ± 9.0	0.14
Mitral annular dynamics			
Mitral annular area (systolic, cm^2)	7.0 ± 1.5	3.7 ± 1.2	0.01
Mitral annular systolic contraction (%)	13.1 ± 11.2	13.3 ± 7.2	0.98
Annular height to commissure width ratio (%)	27.0 ± 2.2	36.8 ± 3.9	0.02

Table 4

Enhanced reciprocal constraint of left ventricular outflow tract and mitral valve annulus during application of cerclage tension, n=10.

		Baseline	Tension	*p*
Left ventricular outflow tract (LVOT) diameter (cm)	Systole	2.1 ± 0.4	2.0 ± 0.4	0.047
	Diastole	1.9 ± 0.4	1.5 ± 0.4	<0.001
	Difference	11%	30%	<0.001
Mitral valve annulus (MVA) diameter (cm)	Systole	3.1 ± 0.5	2.5 ± 0.4	<0.001
	Diastole	3.4 ± 0.6	2.9 ± 0.5	<0.001
	Difference	−10%	−14%	<0.001
Combined LVOT and MVA (cm)	Systole	5.2 ± 0.7	4.5 ± 0.6	NS
	Diastole	5.3 ± 0.9	4.4 ± 0.7	NS
	Difference	−3%	1%	NS